

Incorporation of cobalt into ZnO nanoclusters

Igor Ozerov,* Françoise Chabre, and Wladimir Marine†

CRMC-N, UPR 7251 CNRS, Université de la Méditerranée, Case 901, 13288 Marseille Cedex 9, France.

(Dated: March 23, 2022)

The structural, optical and magnetic properties of nanostructured ZnO films co-doped with cobalt and aluminium have been studied. The nanocrystalline films, with cluster sizes in range 50 - 100 nm, were deposited by pulsed laser ablation in a mixed atmosphere of oxygen and helium. The nanocrystallites have the wurtzite structure and are highly oriented with the c-axis perpendicular to the substrate. Both optical and electron spin resonance (ESR) spectroscopy results show the substitutional incorporation of Co^{2+} ions on the Zn site inside the ZnO nanoclusters. The temperature dependence of the ESR spectra follows Curie law corresponding to a paramagnetic material.

PACS numbers: 76.30.-v, 78.55.Et, 81.05.Ys, 81.15.Fg

Keywords: Zinc oxide; Nanoclusters; Cobalt; Laser ablation; Electron spin resonance

I. INTRODUCTION

Recently, diluted magnetic semiconductors (DMS) and their nanostructures have attracted a lot of attention because of their potential applications in magneto-electrical and magneto-optical devices [1, 2]. Among the other DMS, ZnO is especially interesting because the valence and ionic radii of the cations matches those of the magnetic transition metals. This fact allows ZnO doping at high concentrations of magnetic ions. Moreover, some recent theoretical [3] and experimental [4, 5, 6, 7] reports have shown the room temperature ferromagnetism in ZnO films highly doped with magnetic impurities. It is predicted that n-type co-doping should reinforce the ferromagnetic ordering [3, 4]. Two principal approaches are used to introduce the transition metal ions into semiconductor materials. First, the magnetic impurities are implanted into the host matrices [8]. Second, the magnetic elements are introduced during the growth [9]. The second method is preferable for the growth of nanostructures. In low dimension nanoscale systems, the surface is widely developed. If the magnetic impurities are located at the surface of the nanoclusters, they are subjected to a stochastic crystalline field that is hardly controllable. Therefore, growth techniques should allow the control of both the size of nanoclusters and the distribution of magnetic impurities inside the clusters.

Recently, we have developed a method for synthesizing pure ZnO nanoclusters with a low size dispersion by pulsed laser ablation in an atmosphere of O_2 and He [10]. In this paper we extend this method to the synthesis of ZnO nanoclusters co-doped with cobalt and aluminium. The optical and magnetic properties of the nanocrystalline, heavily doped $\text{Zn}_{1-x}\text{Co}_x\text{O}:\text{Al}$ films are discussed.

II. EXPERIMENTAL

The targets for film deposition were prepared by mixing in appropriate proportions of pure ZnO, Co_3O_4 and Al_2O_3 powders, cool pressing in the atmospheric air, and by sintering at a temperature of 550°C for 24 hours. Two series of targets were used for the deposition of films having different Al contents (10^{19} and 10^{20} cm^{-3}). Both series contained targets with three different concentrations of Co: 1, 5 and 10 at.%.

The target was placed on a rotating holder inside a stainless steel vacuum chamber evacuated by a turbomolecular pump. After pumping the chamber down to approximately 2×10^{-7} mbar, a continuous flux of oxygen mixed with helium was introduced into the chamber as an ambient. Differential pumping ensured a constant gas flow with controlled partial pressures (4 mbar of oxygen and 1.5 mbar of helium) during the film deposition. The silica substrate was placed in front of the target and kept at a temperature in range $380 - 450^\circ\text{C}$. The ablation was performed by a beam of pulsed ArF* laser ($\lambda = 193$ nm, pulse duration 15 ns, FWHM) focused onto the target with an incident angle of 45° at a fluence of 3.5 J/cm^2 .

The crystalline structure of the obtained films was analyzed by X-ray diffraction (XRD) with $\text{Cu K}\alpha$ source. The size and shape of nanoclusters, as well as the film morphology were determined by scanning electron microscopy (SEM).

Room temperature optical transmission measurements at near-normal incidence were performed in the photon energy region from 1.4 to 4.2 eV. We used a deuterium lamp as the light source and a cooled photo-multiplier in photon counting mode linked to a grating monochromator for the detection of the spectra.

The magnetic properties were studied by electron spin resonance (ESR) measurements using X-band Bruker EMX spectrometer equipped with an Oxford Instruments helium-flow cryostat (4.2 K - 300 K).

*Electronic address: ozerov@crmcn.univ-mrs.fr

†Electronic address: marine@crmcn.univ-mrs.fr

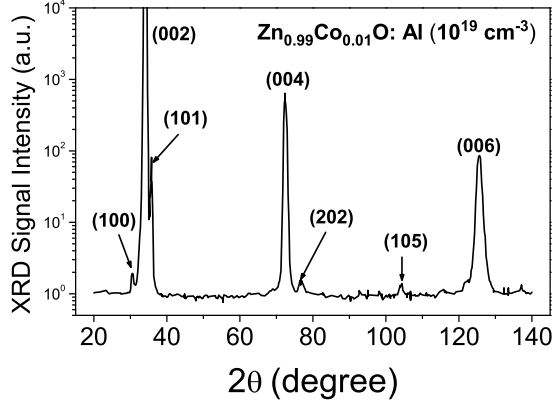


FIG. 1: $\theta - 2\theta$ X-Ray diffraction pattern of a film of $\text{Zn}_{0.99}\text{Co}_{0.01}\text{O}:\text{Al}$ (10^{19}cm^{-3}). The crystalline planes of the wurtzite structure are indicated.

III. RESULTS AND DISCUSSION

The XRD results showed that nanostructured films are crystallized in the wurtzite structure (figure 1). All films are preferentially oriented with the c-axis perpendicular to the substrate surface. Even in the case of amorphous substrates, the c-axis orientation of the films is favorable energetically because of polarity of oxygen- and zinc-terminated (0001) atomic planes of wurtzite structure [10]. However, several crystallites have orientations different from the preferential one (fig. 1). Unlike very recent reports [8, 11], no secondary phase highly doped with cobalt was detected.

SEM images of various samples show that the film surface morphology weakly depends on the deposition temperature in the range from 380 to 450°C and on the proportion of aluminium used. In all cases considered, the

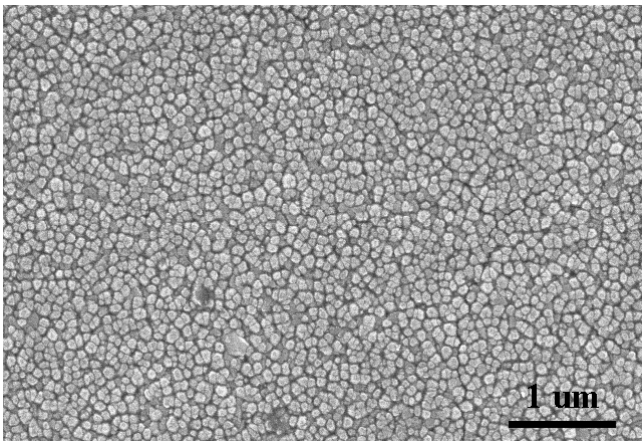


FIG. 2: Typical Scanning Electron Microscopy image of $\text{Zn}_{0.95}\text{Co}_{0.05}\text{O}:\text{Al}$ (10^{19}cm^{-3}) film.

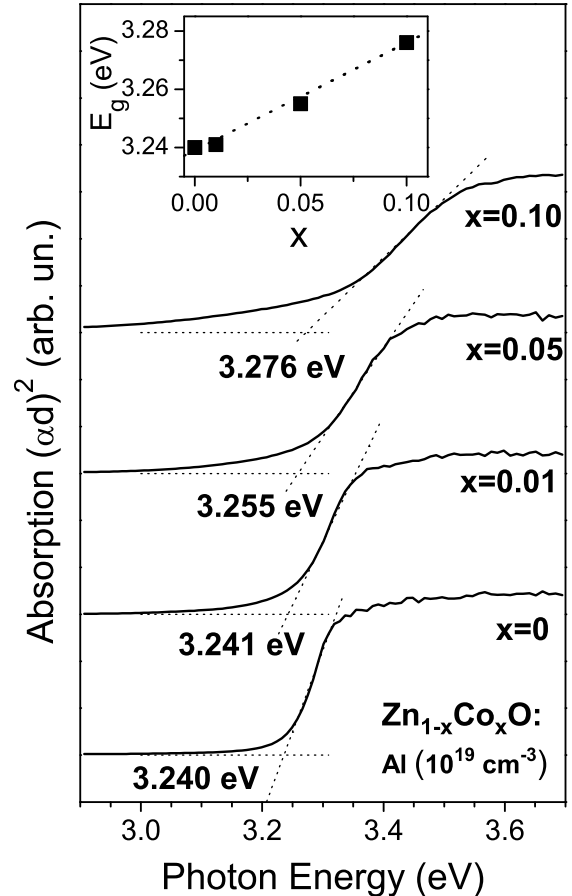


FIG. 3: Optical absorption spectra of $\text{Zn}_{1-x}\text{Co}_x\text{O}:\text{Al}$ (10^{19}cm^{-3}) films for $x = 0, 0.01, 0.05$ and 0.1 . The dotted lines represent linear fits in the band edge region. The inset shows the increase of the bandgap with Co concentration.

distribution of clusters is homogeneous on the surface (figure 2). The main factor driving a difference in the film roughness is the amount of cobalt: the mean size of the clusters decreases as the Co content increases (from 100nm for 1 at. % to 40nm for 10 at.% of cobalt). Chemical analysis by X-ray fluorescence indicates a good agreement between the amount of cobalt used in the targets and the one effectively found in the films.

The obtained films are homogeneous, transparent and have a slight green color of “Rinnmans green” pigment. The intensity of the green color increases with cobalt content. From the calibrated deposition rates, we estimated the thickness of the films to be approximately 1 μm [10].

Figure 3 shows the absorption spectra of the films at room temperature in the photon energy range close to the fundamental absorption edge of ZnO. The absorbance of a pure nanocrystalline ZnO film is given for comparison.

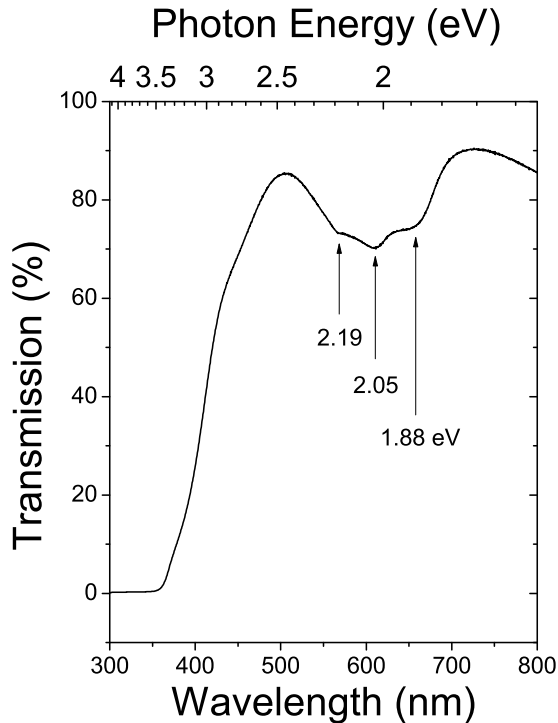


FIG. 4: Optical transmission spectra of Co-doped ZnO films. The d-d transitions in a Co^{2+} ion are indicated with arrows.

Zinc oxide is a direct gap semiconductor. Thus for allowed interband transitions at photon energies above the band gap E_g , the absorption coefficient depends on the photon energy $h\nu$ as follows: $\alpha(h\nu) \sim \sqrt{h\nu - E_g}$. Consistent with the behavior of a direct gap, the absorption spectra are plotted as $(\alpha \cdot d)^2$, where d is the film thickness. The high-energy parts of the absorption spectra were fitted with the linear function (see fig. 3). The extrapolation of this line up to zero absorption gives a value of the direct band gap. We found that E_g increases linearly with increasing Co concentration from 3.240 eV for pure ZnO up to 3.276 eV for $\text{Zn}_{0.9}\text{Co}_{0.1}\text{O}$ (inset in Fig. 3). These results are in disagreement with the gap narrowing with increase in Co for $\text{Zn}_{1-x}\text{Co}_x\text{O}$ doped at extremely high concentrations reported in [6] (x varied from 0.08 to 0.22) and in [12] ($x = 0.1 - 0.4$). The values for E_g reported in [6, 12] approach that reported for CoO in [13]. On the contrary, Yoo et al. [14] reported the increase of E_g in ZnCoAlO films with increase of Co and Al concentrations at moderate doping levels. Thus, the exact nature of the gap in the highly Co-doped ZnO films remains uncertain. The absorption is also present for the photon energies below the fundamental absorption edge (fig. 3) and it becomes stronger with increasing dopant concentration. A strong sp-d exchange interaction between the band states and localized d-electrons reported in Co-doped ZnO from magneto-optical measurements

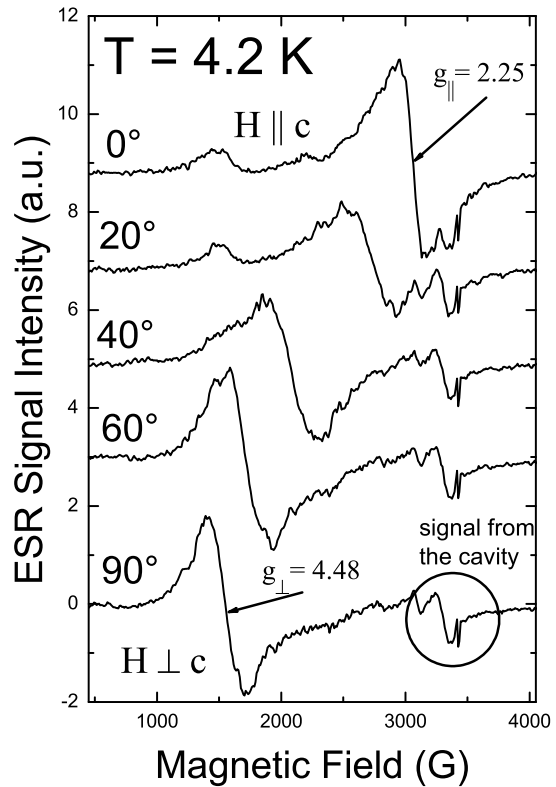


FIG. 5: X-band ESR spectra of a $\text{Zn}_{0.9}\text{Co}_{0.1}\text{O} : \text{Al}$ nanocrystalline film. The concentration of Al is 10^{19} cm^{-3} . The temperature was 4.2 K.

[15] is likely responsible for this absorption tail expanding below the band gap energy.

The optical transmission in wide spectral range is shown in fig. 4. Three absorption bands situated at the photon energies of 1.88, 2.05 and 2.19 eV (shown by arrows in fig. 4) were identified as d-d transitions in Co^{2+} ions situated in the site with a crystalline field of tetrahedral symmetry [16]. These transitions were also observed in highly doped ZnCoO films [6, 12, 14]. However, these bands are large and badly resolved at room temperature, and they can be overlapped with the transitions provided by Co in octahedral symmetry sites [13] or by absorption bands in Co_3O_4 [17] situated between 1.5 and 2.5 eV. Thus, more local methods like ESR should be used to confirm the proper substitutional doping of Co into Zn sites.

Typical ESR spectra of $\text{Zn}_{1-x}\text{Co}_x\text{O}$ nanoclusters are shown in fig. 5. The measurements have been performed at a temperature of 4.2 K by rotating the magnetic field in the plane parallel to the sample surface normal. The spectra contain only one anisotropic resonance line with a Lorentzian shape. The lowest resonance field is obtained for the direction of the magnetic field perpendic-

ular to the [001] direction of the wurtzite structure, and the highest one corresponds to the parallel configuration. Taking \mathbf{x} and \mathbf{z} axes in the rotation plane, \mathbf{z} being parallel to [001] direction, the observed resonance transition is described by the following effective spin Hamiltonian [18]:

$$\mathcal{H}^{eff} = g_{\parallel}^{eff} \beta H S_z^{eff} \cos \theta + g_{\perp}^{eff} \beta H S_x^{eff} \sin \theta \quad (1)$$

where β is the Bohr magneton, H is the magnetic field, g_{\parallel}^{eff} and g_{\perp}^{eff} are the effective values of the g tensor, $S_{z,x}^{eff}$ are the projections of the effective spin and θ is the angle between magnetic field and \mathbf{z} axis. For the observed transition, taking $S^{eff} = 1/2$, we obtain the values $g_{\parallel}^{eff} = 2.25$ and $g_{\perp}^{eff} = 4.48$ (fig. 5).

In the ZnO wurtzite structure, the lowest state 4F of the $3d^7$ Co^{2+} ion is split by the tetrahedral crystal field, 4A_2 being the ground state [16]. The trigonal component of the crystal field splits the ground state 4A_2 corresponding to spin $S = 3/2$ into two Kramers doublets, the lower being $S = \pm 1/2$, and the higher $S = \pm 3/2$. The following Hamiltonian takes the axial crystalline field into account [18, 19]:

$$\mathcal{H} = g_{\parallel} H \beta S_z \cos \theta + g_{\perp} H \beta S_x \sin \theta + D[S_z^2 - \frac{1}{3}S(S+1)] \quad (2)$$

where spin $S = 3/2$ and 2D corresponds to zero-field splitting. The Hamiltonian (1) can be obtained from (2) by assuming $D > 0$ and $|D| \gg \beta H$. The effective g -factor values are: $g_{\parallel}^{eff} = g_{\parallel}$ and $g_{\perp}^{eff} = 2g_{\perp}(1 - \frac{3(g_{\perp}\beta H)^2}{16D^2}) \approx 2g_{\perp}$ [19]. Thus, the only observed transition corresponds to $| - 1/2 \rangle \rightarrow | + 1/2 \rangle$ absorption in the lower Kramers doublet. The transitions between doublets can not be achieved in the available magnetic field range because of the large zero-field splitting 2D [19, 20, 21].

The angular dependence of the spectra of the Co^{2+} ions confirms the hypothesis of substitutional incorporation of dopant in zinc sites. No signal with other symmetry was detected. In the spectra of several samples a low intensity peak at 1555 G was observed for $H \parallel c$ (fig. 5). This transition is due to minority nanocrystallites with the orientations different from that of the main part of the film which is oriented with the c -axis perpendicular to the substrate. This observation is in agreement with the results of XRD experiments (fig. 1).

The width ΔH_{pp} of the Co^{2+} ESR resonance line is independent on the temperature and varies with cobalt concentration from 250 G for $\text{Zn}_{0.99}\text{Co}_{0.01}\text{O}$ to 360 G for $\text{Zn}_{0.90}\text{Co}_{0.10}\text{O}$ in the perpendicular configuration $H \perp c$. These line width values can not be explained by a non-resolved hyperfine structure from ^{59}Co (nuclear spin 7/2, 100%), the components of the hyperfine tensor being too small $A_{\parallel} = 16.11 \times 10^{-4} \text{ cm}^{-1}$ and $A_{\perp} = 3.00 \times 10^{-4} \text{ cm}^{-1}$ [19, 20]. The line width increased due to dipole-dipole interactions. We estimate the dipole-dipole broadening from $W_{dip-dip} = -(\mu H_{dip}) \approx (g\beta S)^2 N$, where spin $S = 3/2$ and N is cobalt concentration. $W_{dip-dip}$ is larger than 200 Gauss for typical concentrations of cobalt we used, that is consistent with the observed line width. No expected exchange narrowing was observed with an increase in concentration.

If the line width does not vary with the temperature, the spin susceptibility χ is reciprocal to the amplitude of the ESR signal [18]. For all the films we deposited, χ follows a Curie law $\chi \propto 1/T$, where T is the temperature. This behavior shows that the samples are paramagnetic, meaning that no high-temperature ferromagnetism is observed in the Co-doped ZnO nanoclusters.

IV. CONCLUSIONS

We have developed a method of synthesis of high quality nanostructured ZnO films doped with Co and Al. The sizes and crystalline quality are controlled by the laser parameters (fluence) and by the ambient gas pressure. The films are constituted by nanocrystallites with wurtzite structure, oriented with the c -axis perpendicular to the substrate. The optical and radiospectroscopic measurements show the homogenous distribution of the cobalt ions in substitution of zinc ions inside the nanoclusters. The magnetic susceptibility follows the Curie law characteristic for a paramagnetic material.

Acknowledgments

It is a pleasure to thank S. Nitsche for the SEM measurements, as well as V. Safarov, J. Marfaing and A. Stepanov for useful discussions.

[1] H. Ohno, Science **281** (1998) 951.

[2] S.J. Pearton, C.R. Abernathy, M.E. Overberg, G.T. Thaler, D. P. Norton, N. Theodoropoulou, A.F. Hebard, Y.D. Park, F. Ren, J. Kim, L. A. Boatner, J. Appl. Phys. **93**, 1 (2003).

[3] H. Katayama-Yoshida, K. Sato, Physica B **327**, 337

(2003).

[4] K. Ueda, H. Tabata, T. Kawai, Appl. Phys. Lett. **79**, 988 (2001).

[5] W. Prellier, A. Fouchet, B. Mercey, Ch. Simon, B. Raveau, Appl. Phys. Lett. **82**, 3490 (2003).

[6] K.J. Kim, Y.R. Park, Appl. Phys. Lett. **81**, 1420 (2002).

- [7] K. Rode, A. Anane, R. Mattana, J.-P. Contour, O. Durand, R. LeBourgeois, *J. Appl. Phys.* **93**, 7676 (2003).
- [8] D.P. Norton, M.E. Overberg, S.J. Pearton, K. Pruessner, J.D. Budai, L.A. Boatner, M.F. Chisholm, J.S. Lee, Z.G. Khim, Y.D. Park, R.G. Wilson, *Appl. Phys. Lett.* **83**, 5488 (2004).
- [9] D.A. Schwartz, N.S. Norberg, Q.P. Nguyen, J.M. Parker, and D.R. Gamelin, *J. Am. Chem. Soc.* **125**, 13205 (2003).
- [10] I. Ozerov, D. Nelson, A.V. Bulgakov, W. Marine, M. Sentis, *Appl. Surf. Sci.* **212-213**, 349 (2003).
- [11] J.H. Kim, H. Kim, D. Kim, Y.E. Ihm, W.K. Choo, *J. Appl. Phys.* **92**, 6066 (2002).
- [12] S.W. Lim, D.K. Hwang, J.M. Myoung, *Solid State Comm.* **125**, 231 (2003).
- [13] G.W. Pratt Jr., R. Coelho, *Phys. Rev.* **116**, 281 (1959).
- [14] Y.Z. Yoo, T. Fukumura, Z. Jin, K. Hasegawa, M. Kawasaki, P. Ahmet, T. Chikyow, H. Koniuma, *J. Appl. Phys.* **90** 4246 (2001).
- [15] K.Ando, H.Saito, Z. Jin, T.Fukumura, M. Kawasaki, Y. Matsumoto, H. Koinuma, *J. Appl. Phys.* **89**, 7284 (2001).
- [16] P. Koidl, *Phys. Rev. B* **15**, 2493 (1977).
- [17] H. Yamamoto, S. Tanaka, K. Hirao, *J. Appl. Phys.* **93** 4158 (2003).
- [18] A. Abragam, B. Bleaney, *Electron Paramagnetic Resonance of Transition Ions*, Vol. 1, Clarendon Press, Oxford, 1970.
- [19] M. De Wit and T.L. Estle, *Bull. Am. Phys. Soc.* **6**, 445 (1961).
- [20] N. Jedercy, H.J. van Bardeleben, Y. Zheng, J.L. Cantin, *Phys. Rev. B* **69**, 041308(R) (2004).
- [21] S. Isber, M. Averous, Y. Shapira, V. Bindilatti, A.N. Anisimov, N.F. Oliveira Jr, V.M. Orera, M. Demianiuk, *Phys. Rev. B* **51**, 15211 (1995).